AAS 13-364

ONLINE ATTITUDE DETERMINATION OF A PASSIVELY MAGNETICALLY STABILIZED SPACECRAFT

Roland Burton[*], Stephen Rock[†], John Springmann[‡], and James Cutler[§]

An online attitude determination filter is introduced that is capable of estimating the attitude of a passively magnetically stabilized spacecraft to within about five degrees accuracy using only an estimate of the solar vector. This filter enables nano satellites to perform onboard attitude determination even when no dedicated attitude sensors are installed, instead relying only on the electrical currents from body mounted solar panels. The online attitude filter is applied in post processing to orbital data from NASA Ames Research Center's O/OREOS and the University of Michigan's RAX-1 spacecraft.

INTRODUCTION

On large spacecraft, high precision attitude determination can be performed using high performance sensors such as star trackers and inertial grade gyros. On nano satellites, however, such instrumentation is not available due to small budgets for mass, volume and power. Furthermore, any attitude sensor that is used will take away valuable budget from the science payload. Consequently it is desirable to be able to perform attitude determination on a nano satellite using few, small sensors.

A candidate minimal sensor set would be the spacecraft's own solar panels. As all satellites require electrical power, they already have solar panels. Thus, no additional components are being added to the spacecraft, and no additional mass, volume or power budget is being used. From differential solar panel currents, an estimate of the solar vector can be obtained, and this can be used to perform attitude determination.

In this paper an online attitude filter is presented that can estimate the attitude of a nano satellite to around 5^{o} precision, using only an estimate of the solar vector. The filter is a derivative of the multiplicative extended Kalman filter (MEKF).[1]

A MEKF was chosen to keep the computational burden low, as nano satellites typically have limited onboard processing capabilities. Each measurement update only requires the inversion of a 6×6 matrix. The MEKF presented in this paper is a new derivation, as existing published implementations rely on the presence of gyros, and only include the kinematics of the spacecraft. As the desire was to perform attitude determination using only an estimate of the solar vector, a full attitude dynamics model of the spacecraft needed to be incorporated into the MEKF.

[*]Stanford University
[†]Prof.,Stanford University
[‡]University of Michigan
[§]Prof., University of Michigan

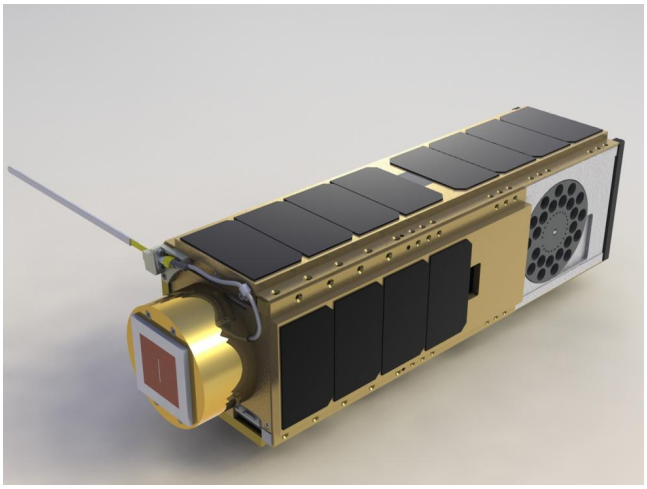

(a) O/OREOS (NASA)

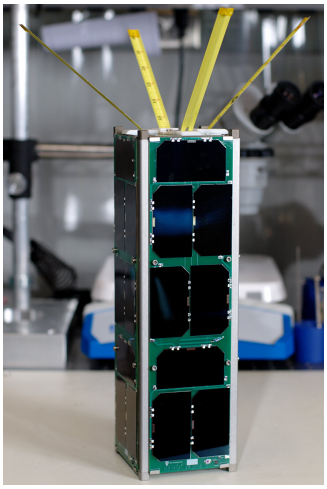

(b) RAX-1 (University of Michigan)

Figure 1. 3U CubeSat nano satellites

The attitude determination algorithm presented in this paper, that only requires an estimate of the solar vector, would still have utility in a nano satellite that contained additional dedicated attitude sensors, such as magnetometers or gyros. If those additional sensors were to fail, the algorithm would provide a fall back attitude determination capability that may allow the original mission to still be performed. Furthermore, the new derivation allows the MEKF to be applied to any set of measurements without significant modification. Even in the case where gyros are available, the filter presented could improve performance when the gyros are noisy, as is often the case with the MEMS gyros commonly used on nano satellites.

This paper starts with a brief overview of the quaternion notation and algebra used in the derivation of the MEKF. A rotational dynamics model for a passively magnetically stabilized nano satellite is developed, and the measurement model, an estimate of the solar vector, is then developed. A brief review of the existing MEKF implementations is given, and then a new implementation is derived that includes spacecraft dynamics. Finally results from applying the new MEKF to flight data from the O/OREOS and RAX-1 spacecraft are presented.

QUATERNION NOTATION

This section provides a brief overview of the quaternion notation used throughout this work. As is common practice in the astrodynamics community, the attitude of the spacecraft will be represented by a unit quaternion. The quaternion notation adopted in this work borrows heavily from that used by Crassidis et al.[2]

The unit quaternion is a four-parameter vector of unit length, partitioned into a three-component vector and a scalar, as defined in Equations (1) and (2). In this work the "scalar last" convention is used, but the reader should be alerted that the scalar can also be the first component and so care

must be taken when consulting other references.

$$q \equiv \begin{bmatrix} \varrho \\ q_4 \end{bmatrix} \tag{1}$$

$$\varrho \in \mathbb{R}^3, q_4 \in \mathbb{R}, \|q\|_2 = 1 \tag{2}$$

The unit quaternion can be related to the angle-axis representation of a generalized rotation as in Equation (3), where e is the axis of rotation, and ϕ is the angle of rotation about that axis.

$$\varrho = e \sin\left(\frac{\phi}{2}\right) \qquad q_4 = \cos\left(\frac{\phi}{2}\right) \tag{3}$$

From Equation (3) it can be seen that $-q$ and q represent the same rotation, and that the inverse rotation is given by Equation (4).

$$q^{-1} \equiv \begin{bmatrix} -\varrho \\ q_4 \end{bmatrix} \tag{4}$$

Two identities are introduced in Equation (5) that will be useful when manipulating quaternions algebraically,

$$\Xi(q) \equiv \begin{bmatrix} q_4 I_{3\times 3} + [\varrho\times] \\ -\varrho^{\mathrm{T}} \end{bmatrix}, \quad \Psi(q) \equiv \begin{bmatrix} q_4 I_{3\times 3} - [\varrho\times] \\ -\varrho^{\mathrm{T}} \end{bmatrix} \tag{5}$$

where $[\varrho\times]$ denotes the usual skew-symmetric cross-product matrix defined in Equation (6).

$$[\varrho\times] \equiv \begin{bmatrix} 0 & -q_3 & q_2 \\ q_3 & 0 & -q_1 \\ -q_2 & q_1 & 0 \end{bmatrix} \tag{6}$$

The direction cosine matrix, A, can be computed from the unit quaternion by using Equation (7).

$$A(q) = \left(q_4^2 - \|\varrho\|^2\right) I_{3\times 3} + \varrho\varrho^{\mathrm{T}} - 2q_4[\varrho\times] = \Xi^{\mathrm{T}}(q)\Psi(q) \tag{7}$$

Quaternion multiplication is used to combine rotations. In contrast to the convention established by Hamilton,[3] this work will adopt an order of rotations that follows that of direction cosine matrices, as shown in Equation (8). The product of two quaternions can be computed using Equation (9).

$$A(q')A(q) = A(q' \otimes q) \tag{8}$$

$$q' \otimes q = \begin{bmatrix} \Psi(q') & q' \end{bmatrix} q = \begin{bmatrix} \Xi(q) & q \end{bmatrix} q' \tag{9}$$

Quaternion multiplication can be used to rotate a vector. Letting unit quaternion q represent the rotation from the inertial frame to the body frame, a vector x expressed in the inertial frame can be computed in the body frame using Equation (10) via the direction cosine matrix, or directly using quaternion multiplication with Equation (11).

$$x_{\text{body}} = A(q)x_{\text{inertial}} \tag{10}$$

$$\begin{bmatrix} x_{\text{body}} \\ 0 \end{bmatrix} = q \otimes \begin{bmatrix} x_{\text{inertial}} \\ 0 \end{bmatrix} \otimes q^{-1} \tag{11}$$

In this work, when a vector and a unit quaternion are multiplied together, it will be assumed that the vector will be suitably augmented. Using this shorthand, Equation (11) can be rewritten as in Equation (12).

$$x_{\text{body}} = q \otimes x_{\text{inertial}} \otimes q^{-1} \tag{12}$$

The attitude kinematics of a body describe how the body's attitude change with time. When using the unit quaternion to represent attitude, the kinematics of a body rotating with an angular rate ω expressed in the body frame are described by Equation (13).

$$\dot{q} = \frac{1}{2} \begin{bmatrix} \omega \\ 0 \end{bmatrix} \otimes q \tag{13}$$

Equation (13) can be written in the shorthand introduced earlier in this Section as in Equation (14).

$$\dot{q} = \frac{1}{2} \omega \otimes q \tag{14}$$

SPACECRAFT DYNAMICS

In this section the dynamics model of a passively magnetically stabilized spacecraft is developed.

Equation (15) is the equation of motion, derived from Euler's Equation, for a passively magnetically stabilized spacecraft. In Equation (15), ω are the body rates, I is the moment of inertia tensor, H the external magnetic field, M the total dipole and T_{dist} external torques, all expressed in the body frame.

$$0 = I\dot{\omega} + \omega \times I\omega + \mu_0(H \times M) - T_{\text{dist}} \tag{15}$$

The torques acting on the spacecraft have deliberately been split between those arising from the passive magnetic stabilization system and those arising from other sources. As can be seen from Table 1, which lists the major torques acting on the nano satellites in this study, these disturbance torques are several orders of magnitude less than those arising from the magnetic system, and will not be modeled.

Torque Source	Nominal Value (Nm)
Magnetic Dipole	7×10^{-4}
Gravity Gradient	7×10^{-8}
Solar Radiation Pressure	2×10^{-8}
Aerodynamic Pressure	2×10^{-9}

Table 1. Torques acting on a 3U nano satellite in a 650 km low Earth orbit

The external magnetic field in the body frame, H, is computed from the assumed known value in an inertial frame using Equation (16), where q is the unit quaternion describing the spacecraft's attitude.

$$H = q \otimes H_{\text{ECI}} \otimes q^{-1} = A(q)H_{\text{ECI}} \tag{16}$$

The external magnetic field in an inertial frame, H_{ECI} can be computed using the IGRF[4] model. It is assumed that the satellite position is known either from onboard GPS, or propagation of the latest TLE using the SGP4[5] propagator.

A passive magnetic stabilization system consists of permanent dipoles that provide alignment to the Earth's magnetic field, and permeable rods that provide damping during the post-separation de-tumble phase. The total dipole, M, can be computed using Equation (17) where M_{P} is the permanent dipole, and B_i and V_i are the induced flux density and the volume of the ith permeable rod.

$$M = M_{\mathrm{P}} + \sum_{i=1}^{m} n_i \frac{B_i(t) V_i}{\mu_0} \tag{17}$$

An attitude determination capability is most important during the science phase of the mission, when the spacecraft is in steady state and the permeable rods are provide minimal damping. During this phase the contribution from the permanent dipole dominates the total dipole, and so it will be assumed that $M \approx M_{\mathrm{P}}$.

Filter performance is dependent on the accuracy of the dynamics model. The parameters of passive magnetic stabilization systems have been shown to be hard to characterize prior to launch.[6,7] More accurate estimates of the parameters can be obtained by performing an on orbit calibration.[8]

ESTIMATING THE SOLAR VECTOR

In this paper it is assumed that the only measurement available is an estimate of the solar vector. This can be obtained from differential solar panel currents, or photodiodes if the spacecraft is so equipped. Figure 2 illustrates the general process, whereby raw readings are taken, scaled based on recent maxima to account for degradation, and then opposing panels inverted, before finally scaling to a unit-length vector.

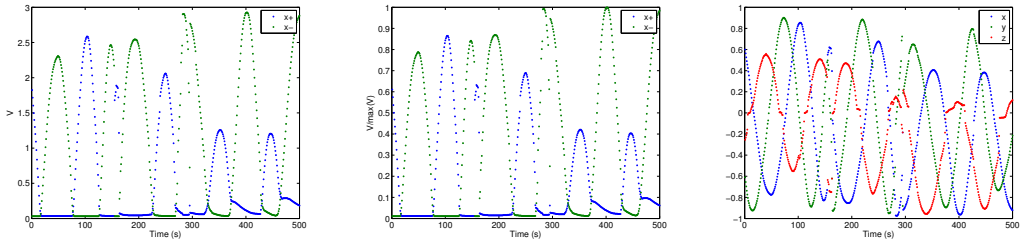

(a) Raw Sensor Readings ($+x$ and $-x$ panels)

(b) Scaled Sensor Readings ($+x$ and $-x$ panels)

(c) Estimated Sun Vector

Figure 2. Example of estimating sun vector from raw sensor readings

As can be seen from Figure 2(c) the final vector estimate is not a clean estimate. Neither solar panel currents nor photodiode voltages are pure cosine estimators. Further readings taken with shallow glancing angles (close to 90^{o} to the surface normal) are especially noisy, leading to data corruption close to zero-crossings. Despite all these problems, as will be seen in the Results section, this estimate is still sufficient for the filter to provide good attitude estimates.

The estimate of the solar vector in the body frame can be related to that in the inertial frame using Equation (18), where q is the unit quaternion describing the spacecraft's attitude.

$$c = q \otimes c_{\mathrm{ECI}} \otimes q^{-1} = A(q) c_{\mathrm{ECI}} \tag{18}$$

The solar vector in an inertial frame is a function of the sun's position in inertial space with respect to the spacecraft, as in Equation (19), and varies predominantly with the time of year.

$$c_{\text{ECI}} = \left(\frac{r_{\text{sun}} - r_{\text{s/c}}}{\|r_{\text{sun}} - r_{\text{s/c}}\|} \right)_{\text{ECI}} \tag{19}$$

THE MULTIPLICATIVE EXTENDED KALMAN FILTER

The multiplicative extended Kalman filter (MEKF) was originally introduced[1] to overcome the problems that occur when attempting to filter quaternions directly. The MEKF introduced a multiplicative error state, which is combined with a deterministic reference quaternion to obtain the true quaternion, as given in Equation (20).

$$q = \delta q(a) \otimes q_{\text{ref}} \tag{20}$$

It is assumed that the error quaternion, $\delta q(a)$ is small and can be parameterized by a three component error vector $a \in \mathbb{R}^3$. The multiplicative state overcomes the problem of maintaing unit quaternion length, and the reduced representation avoids a singular covariance matrix. As the error is assumed small, it is assumed that it remains far from the singularities associated with three-parameter representations of attitude.

Two kinematic equations are required in the MEKF, one in the true state, and one in the reference state, and this introduces a reference angular rate state, ω_{ref}, as given in Equations (21) and (22).

$$\dot{q} = \frac{1}{2}\omega \otimes q \tag{21}$$

$$\dot{q}_{\text{ref}} = \frac{1}{2}\omega_{\text{ref}} \otimes q_{\text{ref}} \tag{22}$$

In the original development of the MEKF,[1] it was assumed that the expected value of the error vector is zero. By taking expectations of both sides of Equation (20), this requires that the reference quaternion is the expected value of the true quaternion, as in Equation (23). To also ensure that $\mathrm{E}[\dot{a}] = 0$, it is required that the reference angular rate is the expected value of the true angular rate, as in Equation (24).

$$\mathrm{E}[q] = \hat{q} = q_{\text{ref}} \tag{23}$$

$$\mathrm{E}[\omega] = \hat{\omega} = \omega_{\text{ref}} \tag{24}$$

When gyros are present, the expected value of the angular rate, $\hat{\omega}$, is given by the current gyro reading and the current estimate of the gyro bias, as in Equation (25).

$$\hat{\omega} = \omega_{\text{gyro}} - \hat{b}_{\text{gyro}} \tag{25}$$

When gyros are not present, the expected value of the angular rates, $\hat{\omega}$, must come from the filter state itself.

When filtering only on kinematics and using gyros, the expectation of ω is conditioned on only one measurement, and performance will be heavily dependent on noise in the gyros. When including dynamics, the expectation is conditioned on all prior measurements, and so filter performance is dependent on how accurate the dynamics model matches the real system.

A MEKF WITH SYSTEM DYNAMICS

In this section a MEKF is developed that uses the full equations of motion of the spacecraft. Instead of introducing reference states, and later equating to expected values of the state, the filter is developed such that the multiplicative error is introduced as a natural extension of the extended Kalman filter to spherical algebras.

In an extended Kalman filter (EKF), the true state, x, is composed of the sum of the expected value of the state, $\hat{x}$, which is estimated, and an error state, Δx, as described in Equation (26). In addition to the expected value of the true state, the covariance of the error state, $\hat{\Sigma}_x$, is also estimated.

$$x = \Delta x + \hat{x} \tag{26}$$

$$\mathrm{E}[\Delta x] = 0 \tag{27}$$

$$\mathrm{E}[\Delta x \Delta x^{\mathrm{T}}] = \hat{\Sigma}_x \tag{28}$$

When filtering on spacecraft dynamics, the state is composed of the attitude, represented by unit quaternion q, and the angular rates in the body frame, ω. As in the EKF, the true state is split into an error state and an estimate of the expected value of the state. As addition of unit quaternions is not defined, a multiplicative error state is used. Equation (26) is replaced by Equations (29) and (30).

$$q = \delta q \otimes \hat{q} \tag{29}$$

$$\omega = \Delta\omega + \hat{\omega} \tag{30}$$

A multiplicative error state would be applicable to any state constrained to unit length, not just the unit quaternion existing in $\mathbb{SO}^3$.

By taking expectations of both sides of Equation (29), it can be seen that the expected value of the error quaternion, $\mathrm{E}[\delta q] = \delta\hat{q}$, is the identity quaternion. The covariance of the error quaternion, $\mathrm{E}[\delta q \delta q^{\mathrm{T}}]$ is expected to be of rank three due to the unit length constraint on any quaternion. To avoid this, the (assumed small) error quaternion will be represented by a three-parameter vector as in Equation (31).

$$\delta q = \delta q(a) \approx \begin{bmatrix} a \\ 1 \end{bmatrix}, \qquad a \in \mathbb{R}^3 \tag{31}$$

The expected value of the error vector, $\mathrm{E}[a] = \hat{a}$, is zero. As a is small, twice the components of a are approximately equal to the Euler angles between the true quaternion q and the expected quaternion $\hat{q}$.

$$a \approx \frac{1}{2} \begin{bmatrix} \phi \\ \theta \\ \psi \end{bmatrix} \tag{32}$$

The direction cosine matrix associated with the error quaternion can be described using Equation (33)

$$A(\delta q(a)) \approx \left(1 - a^{\mathrm{T}} a\right) \mathrm{I}_{3\times 3} + a a^{\mathrm{T}} - 2[a\times] \tag{33}$$

In addition to estimating the expected values of the kinematic state, $(\hat{q}, \hat{\omega})$, the MEKF will also track the error covariance as defined in Equation (34),

$$\hat{\Sigma} = \begin{bmatrix} \hat{\Sigma}_a & \hat{\Sigma}_{a\omega} \\ \hat{\Sigma}_{\omega a} & \hat{\Sigma}_\omega \end{bmatrix} = \begin{bmatrix} \mathrm{E}[aa^{\mathrm{T}}] & \mathrm{E}[a\Delta\omega^{\mathrm{T}}] \\ \mathrm{E}[\Delta\omega a^{\mathrm{T}}] & \mathrm{E}[\Delta\omega\Delta\omega^{\mathrm{T}}] \end{bmatrix} \tag{34}$$

In order to propagate this covariance matrix, time and measurement update equations will need to be derived that include the error vector a.

Time Update:

The system dynamics are given in Equations (35) and (36).

$$\dot{q} = \frac{1}{2}\omega \otimes q \tag{35}$$

$$\begin{aligned} \dot{\omega} =& I^{-1}\left(\mu_0(M_{\mathrm{P}} \times (A(q)H_{\mathrm{ECI}} + \eta_2)) - \omega \times I\omega + \eta_1\right) \\ =& I^{-1}\left(\mu_0(M_{\mathrm{P}} \times (A(\delta q(a))A(\hat{q})H_{\mathrm{ECI}} + \eta_2)) - \omega \times I\omega + \eta_1\right) \end{aligned} \tag{36}$$

The noise term η_1 models unknown disturbance torques, and the noise term η_2 models errors in the IGRF field, including those arising from orbital position errors. Both are assumed isotropic, with standard deviations σ_T and σ_H respectively, as given in Equations (37) and (38).

$$\mathrm{E}[\eta_1] = 0, \quad \mathrm{E}[\eta_1\eta_1^{\mathrm{T}}] = \sigma_T^2 \mathrm{I}_{3\times 3} \tag{37}$$

$$\mathrm{E}[\eta_2] = 0, \quad \mathrm{E}[\eta_2\eta_2^{\mathrm{T}}] = \sigma_H^2 \mathrm{I}_{3\times 3} \tag{38}$$

As in the standard extended Kalman filter, the estimates of the expectation of the state are updated by evaluating Equations (35) and (36) at the expected values of the state, $(\hat{q}, \hat{\omega})$, and assuming zero noise, as in Equations (39) and (40).

$$\dot{\hat{q}} = \frac{1}{2}\hat{\omega} \otimes \hat{q} \tag{39}$$

$$\dot{\hat{\omega}} = I^{-1}\left(\mu_0(M_{\mathrm{P}} \times (A(\hat{q})H_{\mathrm{ECI}})) - \hat{\omega} \times I\hat{\omega}\right) \tag{40}$$

In doing this the implicit assumption that $\mathrm{E}[f(x)] \approx f(\mathrm{E}[x])$ is being made.

As in the standard EKF, the estimate of the covariance is updated using Equation (41). For the MEKF, the Jacobian matrices F and G are defined in Equations (42) and (43). Q is the covariance of the process noise in the system dynamics.

$$\dot{\hat{\Sigma}} = F\hat{\Sigma} + \hat{\Sigma}F^{\mathrm{T}} + GQG^{\mathrm{T}} \tag{41}$$

$$F = \begin{bmatrix} \left.\frac{\partial \dot{a}}{\partial a}\right|_{\hat{q},\hat{\omega}} & \left.\frac{\partial \dot{a}}{\partial \omega}\right|_{\hat{q},\hat{\omega}} \\ \left.\frac{\partial \dot{\omega}}{\partial a}\right|_{\hat{q},\hat{\omega}} & \left.\frac{\partial \dot{\omega}}{\partial \omega}\right|_{\hat{q},\hat{\omega}} \end{bmatrix} \tag{42}$$

$$G = \begin{bmatrix} \left.\frac{\partial \dot{a}}{\partial \eta_1}\right|_{\hat{q},\hat{\omega}} & \left.\frac{\partial \dot{a}}{\partial \eta_2}\right|_{\hat{q},\hat{\omega}} \\ \left.\frac{\partial \dot{\omega}}{\partial \eta_1}\right|_{\hat{q},\hat{\omega}} & \left.\frac{\partial \dot{\omega}}{\partial \eta_2}\right|_{\hat{q},\hat{\omega}} \end{bmatrix} \tag{43}$$

In order to compute the matrix F, an equation in the time derivative of the error vector $\dot{a}$ needs to be derived. To start, the time derivative of Equation (29) is taken:

$$\dot{q} = \delta\dot{q} \otimes \hat{q} + \delta q \otimes \dot{\hat{q}} \tag{44}$$

In Equation (44) the terms for $\dot{q}$ and $\dot{\hat{q}}$ are replaced using Equations (35) and (39).

$$\frac{1}{2}\omega \otimes q = \delta\dot{q} \otimes \hat{q} + \delta q \otimes \frac{1}{2}\hat{\omega} \otimes \hat{q} \tag{45}$$

Equation (45) is post-multiplied by $\hat{q}^{-1}$ to arrive at Equation (46), where the identity $\delta q = q \otimes \hat{q}^{-1}$ has also been used.

$$\delta\dot{q} = \frac{1}{2}\omega \otimes \delta q - \delta q \otimes \frac{1}{2}\hat{\omega} \tag{46}$$

Equation (46) can be rewritten using the quaternion identities introduced in Equation (5) as Equation (47).

$$\delta\dot{q} = \frac{1}{2}\Xi(\delta q)\omega - \frac{1}{2}\Psi(\delta q)\hat{\omega} \tag{47}$$

Equation (48) is another expression for $\delta\dot{q}$, obtained by taking the time derivative of Equation (31).

$$\delta\dot{q} \approx \begin{bmatrix} \dot{a} \\ 0 \end{bmatrix} \tag{48}$$

Expanding out the matrix expressions in Equation (47) and substituting in Equations (31) and (48) gives Equation (49).

$$\begin{bmatrix} \dot{a} \\ 0 \end{bmatrix} \approx \frac{1}{2}\begin{bmatrix} \mathrm{I}_{3\times 3} + [a\times] \\ -a^{\mathrm{T}} \end{bmatrix}\omega - \frac{1}{2}\begin{bmatrix} \mathrm{I}_{3\times 3} - [a\times] \\ -a^{\mathrm{T}} \end{bmatrix}\hat{\omega} \tag{49}$$

Finally, the expression for $\dot{a}$ can be isolated and is given in Equation (50).

$$\dot{a} \approx \frac{1}{2}\left(\omega - \hat{\omega} + a \times (\omega + \hat{\omega})\right) \tag{50}$$

The expression for $\dot{a}$ can be used to compute the Jacobian matrices, F and G , and these are given in Equations (51) and (52). Equation (33) was substituted into Equation (36) when taking partial derivatives with respect to a. When evaluating F at $q = \hat{q}$, note that $a = 0$ also.

$$F = \begin{bmatrix} -[\hat{\omega}\times] & \frac{1}{2}\mathrm{I}_{3\times 3} \\ 2I^{-1}[M_{\mathrm{P}}\times][A(\hat{q})H_{\mathrm{ECI}}\times] & I^{-1}\left(-[\hat{\omega}\times]I + [I\hat{\omega}\times]\right) \end{bmatrix} \tag{51}$$

$$G = \begin{bmatrix} 0 & 0 \\ I^{-1} & I^{-1}[M_{\mathrm{P}}\times] \end{bmatrix} \tag{52}$$

Although Equation (41) can be integrated as written, maintaing $\hat{\Sigma}$ to be positive definite can be problematic. Instead the estimate of the covariance matrix can be updated using a state transition matrix as in Equation 53, which maintains $\hat{\Sigma} > 0$.

$$\hat{\Sigma}(t_f) = \Phi_{t_i,t_f}\hat{\Sigma}(t_i)\Phi_{t_i,t_f}^{\mathrm{T}} + \int_{t_i}^{t_f} G(\tau)Q(\tau)G^{\mathrm{T}}(\tau)d\tau \tag{53}$$

The state transition matrix Φ is computed using Equation (54).

$$\begin{aligned}\Phi_{t_i,t_f} =& \exp(F(t_i)(t_f - t_i)) \\ \approx& \mathrm{I}_{n\times n} + F(t_i)(t_f - t_i)\end{aligned} \tag{54}$$

Measurement Update:

The measurement function is given in Equation 55, where c_{ECI} denotes the solar unit vector from the spacecraft to the sun expressed in an inertial frame.

$$\begin{aligned}y = h(q,\omega,\nu) =& A(q)c_{\text{ECI}} + \nu \\ =& A(\delta q(a))A(\hat{q})c_{\text{ECI}} + \nu\end{aligned} \tag{55}$$

It is assumed that the noise ν is isotropic with standard deviation σ_c.

$$\mathrm{E}[\nu] = 0, \qquad \mathrm{E}[\nu\nu^{\mathrm{T}}] = \sigma_c^2 \mathrm{I}_{3\times 3} \tag{56}$$

The expected measurement at time t_k is computed using Equation (57) where again there is an explicit assumption that $\mathrm{E}[f(x)] \approx f(\mathrm{E}[x])$.

$$\hat{y}(t_k) = \hat{h}(\hat{q}(t_k), \hat{\omega}(t_k)) = A(\hat{q}(t_k))c_{\text{ECI}} = \hat{c}(t_k) \tag{57}$$

When a measurement $\tilde{y}_k = \tilde{c}_k$ arrives at time t_k, then the state estimates are updated using Equations (58) through (62).

$$K_k = \hat{\Sigma}(t_k)^- H_k^{\mathrm{T}} \left(H_k \hat{\Sigma}(t_k)^- H_k^{\mathrm{T}} + J_k R_k J_k^{\mathrm{T}} \right) \tag{58}$$

$$\begin{bmatrix} a_k \\ \Delta\omega_k \end{bmatrix} = K_k \left(\tilde{c}_k - \hat{h}(\hat{q}(t_k)^-, \hat{\omega_k}(t_k)^-) \right) \tag{59}$$

$$\hat{q}(t_k)^+ = \delta q(a_k) \otimes \hat{q}(t_k)^- \tag{60}$$

$$\hat{\omega}(t_k)^+ = \Delta\omega_k + \hat{\omega}(t_k)^- \tag{61}$$

$$\hat{\Sigma}(t_k)^+ = \left(\mathrm{I}_{6\times 6} - K_k H_k\right) \hat{\Sigma}(t_k)^- \tag{62}$$

The Jacobian matrices H_k and J_k are defined in Equations (63) and (64).

$$\begin{aligned}H_k =& \left[\frac{\partial h}{\partial a}\Big|_{\hat{q}(t_k)^-, \hat{\omega}(t_k)^-} \quad \frac{\partial h}{\partial \omega_k}\Big|_{\hat{q}(t_k)^-, \hat{\omega}(t_k)^-} \right] \\ =& \left[2[A(\hat{q}(t_k)^-)c_{\text{ECI}}\times] \quad 0_{3\times 3} \right]\end{aligned} \tag{63}$$

$$\begin{aligned}J_k =& \left.\frac{\partial h}{\partial \nu}\right|_{\hat{\omega}(t_k)^-} \\ =& \mathrm{I}_{3\times 3}\end{aligned} \tag{64}$$

In computing the partial derivative of the measurement function h with respect to the error vector a, Equation (33) was used, again evaluated at $a = 0$.

When comparing the measurement update in the MEKF derived above to that in a standard EKF, the difference is in how the state estimate measurement update computed in Equation (59) is applied. In the MEKF the attitude component of the update is applied as a multiplicative update in Equation (60). The angular rate update is applied in the same way as it would be a regular EKF.

SUMMARY OF MEKF EQUATIONS

The MEKF derived in the previous section for a passively magnetically stabilized spacecraft is summarized in Equations (65) through (74).

Initial Conditons:

$$\hat{q}(t_0)^- = \hat{q}_0 \tag{65}$$
$$\hat{\omega}(t_0)^- = \hat{\omega}_0 \tag{66}$$
$$\hat{\Sigma}(t_0)^- = \begin{bmatrix} \sigma_{a_0}^2 \mathrm{I}_{3\times3} & 0_{3\times3} \\ 0_{3\times3} & \sigma_{\omega_0}^2 \mathrm{I}_{3\times3} \end{bmatrix} \tag{67}$$

Measurement Update:

$$R = \sigma_c^2 \mathrm{I}_{3\times3} \tag{68}$$
$$H_k = \begin{bmatrix} 2[A(\hat{q}(t_k)^-)c_{\mathrm{ECI}}\times] & 0_{3\times3} \end{bmatrix} \tag{69}$$
$$K_k = \hat{\Sigma}(t_k)^- H_k^{\mathrm{T}} \left(H_k \hat{\Sigma}(t_k)^- H_k^{\mathrm{T}} + R \right) \tag{70}$$
$$\begin{bmatrix} a_k \\ \Delta\omega_k \end{bmatrix} = K_k \left(\tilde{c}_k - A(\hat{q}(t_k)^-)c_{\mathrm{ECI}} \right) \tag{71}$$
$$\hat{q}(t_k)^+ = \delta q(a_k) \otimes \hat{q}(t_k)^- \tag{72}$$
$$\hat{\omega}(t_k)^+ = \Delta\omega_k + \hat{\omega}(t_k)^- \tag{73}$$
$$\hat{\Sigma}(t_k)^+ = \left(\mathrm{I}_{6\times6} - K_k H_k \right) \hat{\Sigma}(t_k)^- \tag{74}$$

Time Update – State Estimate:

$$\dot{\hat{q}}(t) = \frac{1}{2} \hat{\omega}(t) \otimes \hat{q}(t) \tag{75}$$
$$\dot{\hat{\omega}}(t) = I^{-1} \left(\mu_0 (M_{\mathrm{P}} \times (A(\hat{q}(t)) H_{\mathrm{ECI}}(t))) - \hat{\omega}(t) \times I\hat{\omega}(t) \right) \tag{76}$$
$$\hat{q}(t_k)^- = \hat{q}(t_{k-1})^+ + \int_{t_{k-1}}^{t_k} \dot{\hat{q}}(\tau) d\tau \tag{77}$$
$$\hat{\omega}^-(t_k) = \hat{\omega}(t_{k-1})^+ + \int_{t_{k-1}}^{t_k} \dot{\hat{\omega}}(\tau) d\tau \tag{78}$$

Time Update – Covariance Estimate:

$$F(t) = \begin{bmatrix} -[\hat{\omega}(t)\times] & \frac{1}{2}\mathrm{I}_{3\times3} \\ 2I^{-1}[M_{\mathrm{P}}\times][A(\hat{q}(t))H_{\mathrm{ECI}}(t)\times] & I^{-1}\left(-[\hat{\omega}(t)\times]I + [I\hat{\omega}(t)\times]\right) \end{bmatrix} \tag{79}$$
$$G = \begin{bmatrix} 0_{3\times3} & 0_{3\times3} \\ I^{-1} & I^{-1}[M_{\mathrm{P}}\times] \end{bmatrix} \tag{80}$$
$$Q = \begin{bmatrix} \sigma_T^2 \mathrm{I}_{3\times3} & 0_{3\times3} \\ 0_{3\times3} & \sigma_H^2 \mathrm{I}_{3\times3} \end{bmatrix} \tag{81}$$
$$\Phi_{t_k,t_{k-1}} = \exp(F(t_{k-1})(t_k - t_{k-1})) \tag{82}$$
$$\hat{\Sigma}(t_k)^- = \Phi_{t_k,t_{k-1}} \hat{\Sigma}(t_{k-1})^+ \Phi_{t_k,t_{k-1}}^{\mathrm{T}} + GQG^{\mathrm{T}}(t_k - t_{k-1}) \tag{83}$$

Equations (77) and (78) can be integrated using a Runge-Kutta 4th order algorithm, with time step chosen such that $\|\omega dt\|_2 \ll 1$. The quaternion estimate should be renormalized to unit length every ~ 100 time steps.

DATA SOURCES

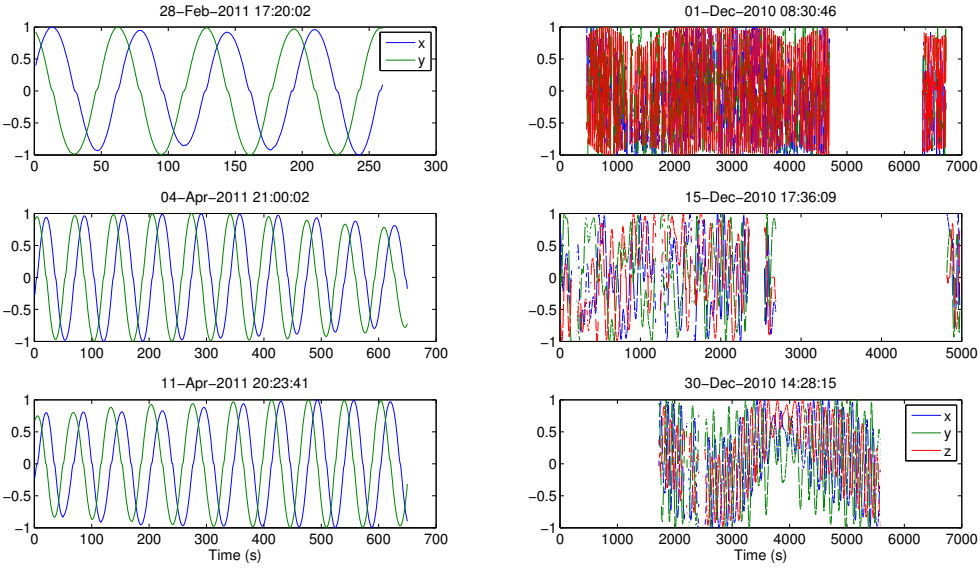

(a) O/OREOS (b) RAX-1

Figure 3. Data Within Each Window

The MEKF developed in the previous section was tested against two sets of actual flight data from the O/OREOS and RAX-1 spacecraft.

The Organism/Organic Exposure to Orbital Stresses (O/OREOS) spacecraft, illustrated in Figure 1(a), is a 3U nano satellite that launched in November 2010 from Kodiak, AK into an approximately 650 km altitude, 72$^{\text{o}}$ low Earth orbit. O/OREOS carried two astrobiology payloads to study the survivability and viability of the space environment to live organisms and organics respectively. The O/OREOS spacecraft passive attitude stabilization system consisted of permanent dipoles along the long axis, and hysteresis rods in the plane perpendicular to the long axis. O/OREOS had no direct onboard attitude sensing, however the spacecraft bus did monitor solar panel currents. After calibrating and filtering the panel currents a rudimentary estimate of the x and y components of the solar vector can be obtained.

Included on the same launch manifest as O/OREOS was the first Radio Aurora Explorer satellite, RAX-1, a 3U CubeSat illustrated in Figure 1(b), that was developed to study magnetic field-aligned plasma irregularities in Earth's ionosphere.[9] The satellite was developed jointly by SRI International and the University of Michigan and the science payload is an ultra high frequency (UHF) radar receiver. Working in conjunction with ground based incoherent scatter radar stations, the purpose of the mission was to improve the understanding of the ionospheric irregularities with the ultimate goal of enabling short-term forecasting. The passive magnetic attitude control system consists of

Term	Description	Value
σ_T	torque disturbances	7.5×10^{-6} Nm
σ_H	errors in magnetic field	2.4×10^{-2} Am^{-1}
σ_c	solar vector measurement noise	4.0×10^{-2}
σ_{a_0}	initial uncertainty in error vector	8.7×10^{-3} rad
σ_{ω_0}	initial uncertainty in angular rate	1.7×10^{-3} rads^{-1}

Table 2. Noise and Uncertainties used in MEKF

four permanent magnets aligned with the long z axis and two strips of HyMu80 soft magnetic material mounted in two axes perpendicular to the permanent magnets. RAX-1 included a full suite of attitude sensors consisting of multiple photodiodes, two three-axis magnetometers, and a three-axis rate gyroscope.[10] To improve the accuracy of the magnetometer and photodiode measurements attitude independent calibration was performed, with an on-orbit magnetometer calibration algorithm developed to mitigate the effect of nearby electronics on the magnetometers, which are embedded in the spacecraft.[11] The calibrated photodiode readings were used to create a reliable estimate of the sun vector in the body frame. In the work described in this paper the calibrated magnetometer data and the gyro data were used solely for verification of filter performance.

Both O/OREOS and RAX-1 recorded data at 1Hz during specific data capture windows. TLE ephemerides were available for both spacecraft with updates occurring about every twenty four hours, leading to maximum orbit propagation errors of a few kilometers.

Several data windows were available for the O/OREOS spacecraft, but each window was typically only a few minutes long. For the RAX-1 spacecraft, only three data windows were available, but these were each around two hours long leading to a rich data set. The solar data from O/OREOS is illustrated in Figure 3(a)., and the data from RAX-1 is illustrated in Figure 3(b).

When applying the MEKF, values for the inertia I and permanent dipole M_{P} were estimated using the batch calibration method referenced previously.[8] For the noise terms required by the filter, Table 2 lists the standard deviations. The estimates of process noise were taken from expected values of disturbance torques, and published errors in the IGRF magnetic field model. Measurement noise was based on observed noise of the estimated solar vector estimate. The initial state uncertainties correspond to 1^{o} angle uncertainty and $0.1^{\mathrm{o}}/\mathrm{s}$ rate uncertainties.

RESULTS

O/OREOS

Figure 4 shows the filter estimates of attitude and attitude rate, using only the solar vector data from the O/OREOS nano satellite.

As the only flight data available from O/OREOS are the solar panel currents, no verification of the attitude estimates are available. Pointing knowledge was estimated by the filter at around 3^{o}, as illustrated in Figure 5.

RAX-1 – Nominal

Figure 6 shows the filter estimates of attitude and attitude rate, using only the solar vector data from RAX-1. The initial estimate of the kinematic state was as generated by the batch dynamics estimation method referenced in the introduction. The "Full Filter" estimate is the attitude profile

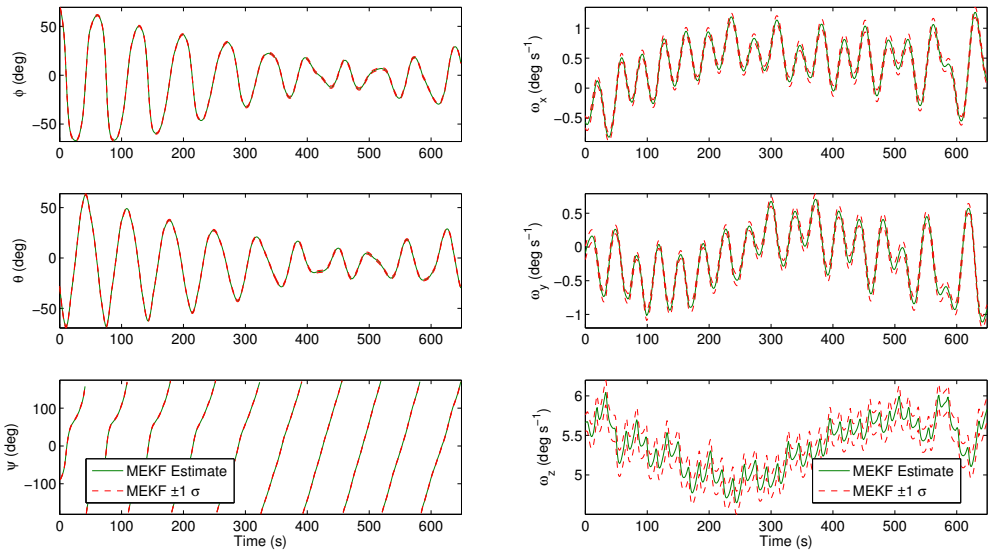

(a) Attitude Estimate (b) Angular Rate Estimate

Figure 4. Performance of the MEKF Attitude Filter – O/OREOS

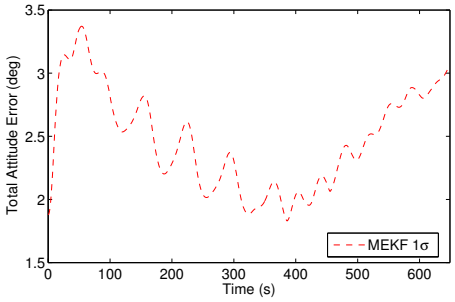

Figure 5. MEKF Pointing Knowledge Error – O/OREOS

as generated by a filter that uses all available bus data, and is used as a truth metric for the attitude of the RAX-1 spacecraft.

Figure 7 shows the attitude and attitude rate errors for the filter, defined as the difference between the MEKF estimate and the "Full Filter". Attitude errors on each axis are typically below 5°, but do rise above 20° for a short period. The filter's estimate of uncertainty, shown as the dashed red $\pm 1\sigma$ line, matches the actual errors well. This is important and means that the filter's estimated uncertainty is an accurate representation of the actual error.

Finally the overall pointing knowledge error is shown in Figure 8. Pointing knowledge is typically around 5°, but with periods of deteriorated performance. The depicted 1σ pointing error is a conservative bound assuming that the largest error of the individual axis errors is distributed isotropically. The poor filter performance starting at around $t = 2000$ s can be explained by examining the geometry of the spacecraft and observations at that time. Figure 9(b) plots the angle between

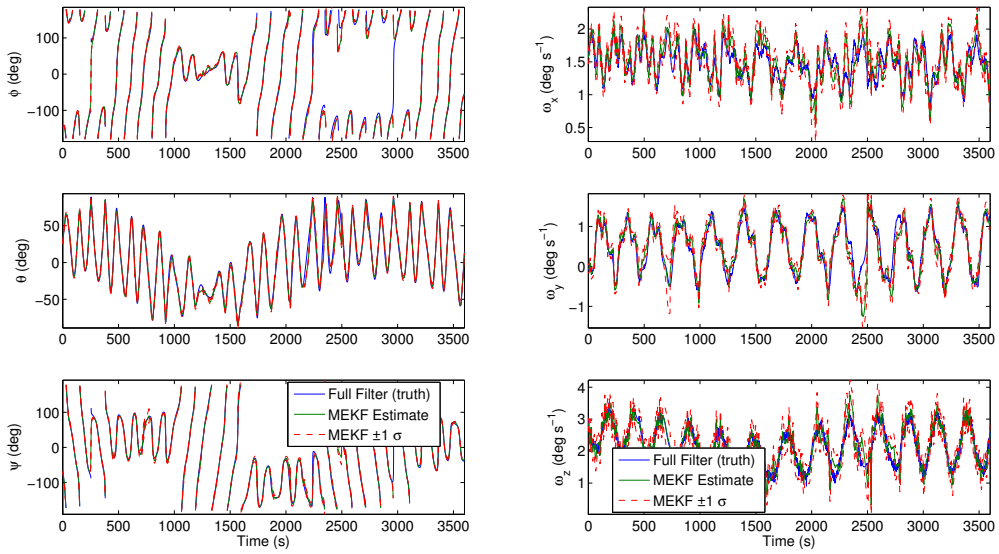

(a) Attitude Estimate

(b) Angular Rate Estimate

Figure 6. Performance of the MEKF Attitude Filter – RAX-1

the spin vector and the solar vector. When these two vectors are aligned, the spin rate cannot be observed, and spacecraft attitude becomes unobservable. When the two vectors are close to aligned, observability decreases, leading to the poor filter performance. Once the geometry improves, the filter is able to return to improved performance. Importantly during this period, the filter error estimate also deteriorates.

RAX-1 – Lost In Space Initialization

The filter is also capable of converging from a lost in space initialization. In such a case the initial estimate of the kinematic state would be the unit quaternion and zero angular rates. A sample convergence is illustrated in Figure 10 and 11(a), showing convergence from an initial pointing error of over 150^{o}.

RAX-1 – Eclipse Performance

Unsurprisingly the online filter is unable to provide good attitude estimates in eclipse. While in eclipse, the filter is entirely reliant on the accuracy of the state estimate just prior to entering eclipse, and the accuracy of the dynamics model. Given typical pointing errors of 5^{o}, it is unlikely that the state estimate on entering eclipse will be good enough to maintain accuracy while no measurements are being received. As the filter is able to converge from a lost-in-space initialization, it is not surprising that the MEKF is able to converge to the correct estimate quickly once re-entering sunlight.

CONCLUSIONS

An online filter has been presented that has been demonstrated to achieve about 5^{o} attitude determination of a passively magnetically stabilized spacecraft using only an estimate of the solar

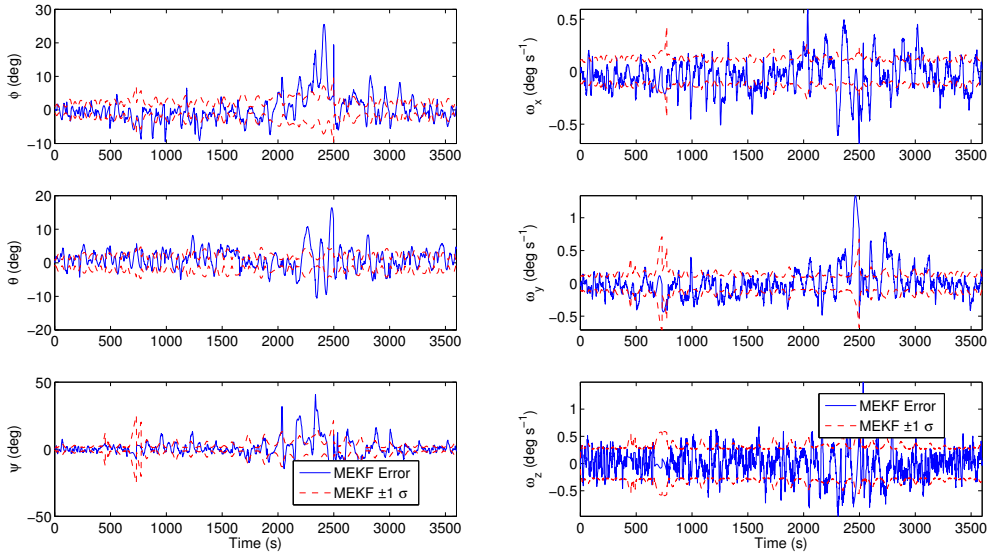

(a) Attitude Errors (b) Angular Rate Errors

Figure 7. Errors of the MEKF Attitude Filter – RAX-1

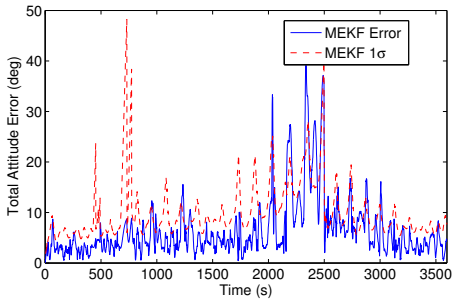

Figure 8. MEKF Pointing Knowledge Error – RAX-1

vector. Filter performance was verified using actual flight data from the O/OREOS and RAX-1 nano satellites. The online filter was a new variant of the multiplicative extended Kalman filter, and incorporates a rotational dynamics model of the spacecraft, allowing the filter to operate without input from gyros.

ACKNOWLEDGEMENTS

The research described in this paper was funded by a grant from the National Aeronautics and Space Administration. Orbital data for the O/OREOS spacecraft was provided by Santa Clara University. Orbital data for the RAX-1 spacecraft was provided by the University of Michigan. RAX-1 was funded by the U.S. National Science Foundation

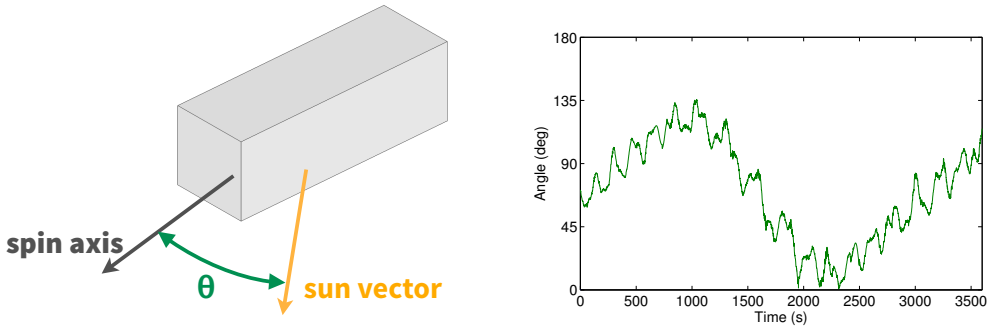

(a) Diagram (b) Angle between spin vector and sun vector

Figure 9. Spacecraft Observation Geometry

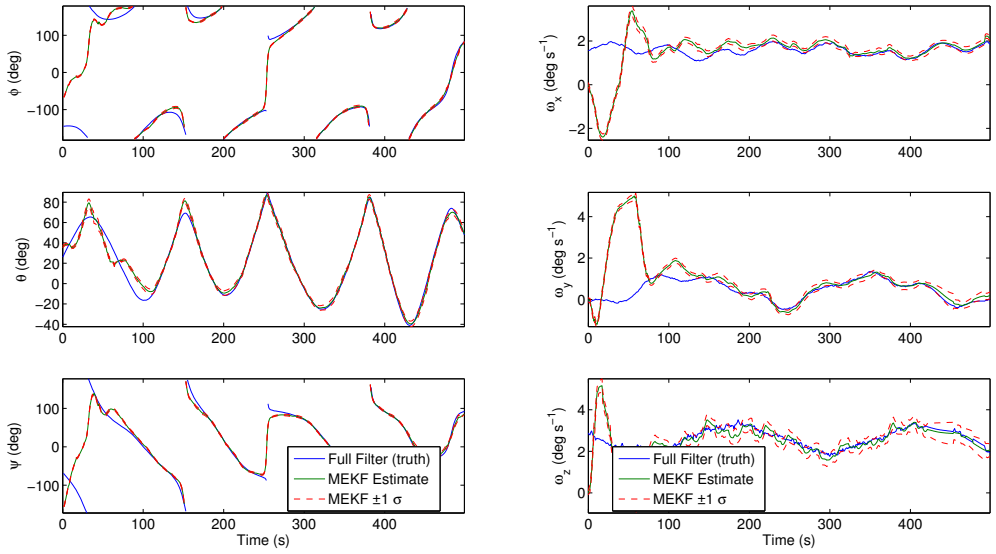

(a) Attitude Estimate (b) Angular Rate Estimate

Figure 10. Convergence of the MEKF Attitude Filter with Lost in Space Initialization – RAX-1

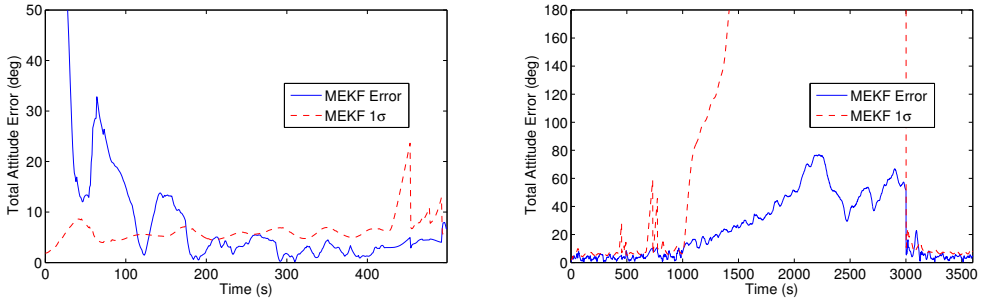

(a) Lost In Space Initialization (b) Performance in Eclipse

Figure 11. MEKF Total Attitude Error – RAX-1

NOTATION

Symbol	Description	Units
μ_0	permeability of free space $= 4\pi \times 10^{-7}$	Hm^{-1}
c	solar unit vector in body frame	
c_{ECI}	solar unit vector in inertial frame	
H	external magnetic field, body frame	Am^{-1}
H_{ECI}	Earth's magnetic field, ECI frame	Am^{-1}
B	induced magnetic flux density in permeable material	T
V	volume of permeable rod material	m^3
M	total dipole of magnetic material	Am^2
M_{P}	permanent dipole in a permanent magnet	Am^2
I	moment of inertia, body frame	kgm^2
T_{dist}	external disturbance torque, body frame	Nm
ω	angular rate, body frame	rad s^{-1}
q	unit quaternion, inertial to body frame	
a	attitude error vector	
Σ	state covariance matrix	

REFERENCES

[1] E. Lefferts, F. Markley, and M. Shuster, "Kalman filtering for spacecraft attitude estimation," *Journal of Guidance, Control, and Dynamics*, Vol. 5, No. 5, 1982, pp. 417–429.

[2] J. Crassidis, F. Markley, and Y. Cheng, "Survey of nonlinear attitude estimation methods," *Journal of guidance control and dynamics*, Vol. 30, No. 1, 2007, p. 12.

[3] S. Hamilton, *Elements of quaternions*. Longmans, Green, & co., 1866.

[4] International Association of Geomagnetism and Aeronomy, Working Group V-MOD. Participating members, C. C. Finlay, S. Maus, C. D. Beggan, T. N. Bondar, A. Chambodut, T. A. Chernova, A. Chulliat, V. P. Golovkov, B. Hamilton, M. Hamoudi, R. Holme, G. Hulot, W. Kuang, B. Langlais, V. Lesur, F. J. Lowes, H. Lühr, S. Macmillan, M. Mandea, S. McLean, C. Manoj, M. Menvielle, I. Michaelis, N. Olsen, J. Rauberg, M. Rother, T. J. Sabaka, A. Tangborn, L. Tøffner-Clausen, E. Thébault, A. W. P. Thomson, I. Wardinski, Z. Wei, and T. I. Zvereva, "International Geomagnetic Reference Field: the eleventh generation," *Geophysical Journal International*, Vol. 183, No. 3, 2010, pp. 1216–1230, 10.1111/j.1365-246X.2010.04804.x.

[5] D. Vallado, P. Crawford, R. Hujsak, and T. Kelso, "Revisiting spacetrack report# 3," *AIAA*, Vol. 6753, 2006, p. 2006.

[6] F. Santoni and M. Zelli, "Passive magnetic attitude stabilization of the UNISAT-4 microsatellite," *Acta Astronautica*, Vol. 65, No. 5-6, 2009, pp. 792 – 803, 10.1016/j.actaastro.2009.03.012.

[7] R. Burton, J. Starek, and S. M. Rock, "A New Method for Simulating the Attitude Dynamics of Passively Magnetically Stabilized Spacecraft," *Proceedings of the 22nd AAS/AIAA Space Flight Mechanics Meeting*, Charleston SC, AAS/AIAA, AAS/AIAA, 2012.

[8] R. Burton, S. M. Rock, J. Springmann, and J. Cutler, "Dual Attitude and Parameter Estimation of Passively Magnetically Stabilized Spacecraft," *Proceedings of the 63rd International Astronautical Congress*, Naples, Italy, International Astronautical Federation, October 2012.

[9] J. Cutler, J. Springmann, S. Spangelo, and H. Bahcivan, "Initial Flight Assessment of the Radio Aurora Explorer," *proceedings of the 25th Annual AIAA/USU Conference on Small Satellites. SSC11-VI-6. Logan, Utah*, 2011.

[10] J. Springmann, A. Sloboda, A. Klesh, M. Bennett, and J. Cutler, "The attitude determination system of the RAX satellite," *Acta Astronautica*, Vol. 75, 2012, pp. 120–135.

[11] J. Springmann, "Attitude-Independent Magnetometer Calibration with Time-Varying Bias," *Proceedings of the 25th Annual Small Satellite Conference*, 2011.